Atmos. Chem. Phys., 25, 5665–5681, 2025
https://doi.org/10.5194/acp-25-5665-2025

Atmospheric Chemistry and Physics
Open Access
EGU

Research article

Modeling simulation of aerosol light absorption over the Beijing–Tianjin–Hebei region: the impact of mixing state and aging processes

Huiyun Du[1,2], Jie Li[1,2,3], Xueshun Chen[1,2], Gabriele Curci[4], Fangqun Yu[5], Yele Sun[1,2], Xu Dao[6], Song Guo[7], Zhe Wang[1,2], Wenyi Yang[8], Lianfang Wei[9], and Zifa Wang[1,2,3]

[1]State Key Laboratory of Atmospheric Environment and Extreme Meteorology, Institute of Atmospheric Physics, Chinese Academy of Sciences, Beijing 100029, China
[2]State Key Laboratory of Atmospheric Boundary Layer Physics and Atmospheric Chemistry (LAPC), Institute of Atmospheric Physics, Chinese Academy of Sciences, Beijing 100029, China
[3]College of Earth and Planetary Sciences, University of Chinese Academy of Sciences, Beijing 100049, China
[4]Department of Physical and Chemical Sciences, University of L'Aquila, L'Aquila, Italy
[5]Atmospheric Sciences Research Center, University at Albany, Albany, NY, USA
[6]China National Environmental Monitoring Centre, Beijing 100012, China
[7]College of Environmental Sciences and Engineering, Peking University, Beijing 100871, China
[8]Center of Environmental Pollution and Greenhouse Gases Co-control, Chinese Academy of Environmental Planning, Beijing 100041, China
[9]Chinese Research Academy of Environmental Sciences, Beijing 100012, China

Correspondence: Jie Li (lijie8074@mail.iap.ac.cn) and Xueshun Chen (chenxsh@mail.iap.ac.cn)

Received: 16 May 2024 – Discussion started: 9 August 2024
Revised: 26 January 2025 – Accepted: 10 March 2025 – Published: 10 June 2025

Abstract. The mixing state and aging characteristics of black carbon (BC) aerosols are the key factors in calculating their optical properties and quantifying their impacts on radiation balance and global climate change. Considerable uncertainty still exists in the absorption properties of BC-containing aerosols and the absorption enhancement (E_{abs}) due to the lensing effect. It is crucial to reasonably represent the mixing of BC with other aerosol components to reduce this uncertainty. In this study, the absorption properties of $PM_{2.5}$ were investigated based on the Nested Air Quality Prediction Modeling System (NAQPMS) with different assumptions of the aerosol mixing state. The absorption coefficient (b_{abs}) is the highest under the assumption of uniform internal mixing, lower under core–shell mixing, and the lowest under external mixing. The result under core–shell mixing is closest to the observations. The aging process and coating thickness were well reproduced by an advanced particle microphysics (APM) module in NAQPMS. Following this, the fraction of embedded BC and secondary component coating on aerosols was used to constrain the mixing state. E_{abs} at 880 nm over the Beijing–Tianjin–Hebei region was 2.0–2.5 under core–shell mixing. When the fraction of coated BC and the coating layer are resolved, E_{abs_880} – caused by the lensing effect – decreases by 30 %–43 % to 1.2–1.7, which is close to the range reported in previous studies. This study highlights the importance of representing the microphysical processes governing the mixing state and aging of BC and provides a reference for quantifying their radiative effects.

Published by Copernicus Publications on behalf of the European Geosciences Union.

1 Introduction

Aerosols have important environmental and climatic effects, affecting not only transportation and public health but also the global radiation balance (Xu et al., 2013; IPCC, 2021). Mainly originating from incomplete burning, black carbon (BC) is an important component of aerosols. The light absorption of BC particles is enhanced by the "lensing effect" of coating, which affects the heating of the atmosphere by BC (Fuller et al., 1999). When BC is coated by hydrophilic components, it can act as cloud condensation nuclei, affecting cloud and rainfall. Previous studies have demonstrated the important radiative forcing effect of BC (Jacobson, 2013; Bond et al., 2013). However, uncertainty in calculating the optical parameters of BC-containing aerosols still exists. It is challenging to quantify the radiative effect of BC.

The mixing state describes the distribution of properties across a population of particles (Riemer et al., 2019). "Externally mixed" means that each particle in a population is composed of a single species. "Internally mixed" means that each particle in the population consists of the same mixture of all chemical species (Stevens and Dastoor, 2019). The concept maps illustrating the mixing state are shown in Matsui et al. (2018, Fig. 4) and Fierce et al. (2017, Fig. 1). The aerosol mixing state is dynamic and changes due to several processes, such as emission, new particle formation, transport, condensation, and coagulation processes (Chen et al., 2023). Purely internal and external mixing states are rare in the real atmosphere (Bondy et al., 2018). In addition, observations have shown that not all BC particles are coated and not all secondary aerosols are coated on BC cores (Li et al., 2016). Transmission electron microscopy has shown that only a proportion of BC aerosols are embedded (Wang et al., 2021b). The fraction of thickly coated BC in Beijing in winter reduced from 48 % to 29 % from 2012 to 2018 (Wu et al., 2021). The presentation of aerosol mixing states in atmospheric models at different scales was highlighted by Riemer et al. (2019). In many models, aerosols are presented in a few modes with assumed size distributions and the same mixing state and compositions in a mode (Liu et al., 2016; Mann et al., 2010). The sectional approach is used in a limited number of models to represent the mixing state (Yu et al., 2012; Matsui et al., 2014; Matsui, 2016; Yu et al., 2015). Furthermore, particle-resolved models can accurately simulate BC mixing states, but they are applied only to box and single-column models due to the high computational cost (Riemer et al., 2009; Zaveri et al., 2010; Curtis et al., 2017). Yao et al. (2022) verified the important yet complicated role of mixing state in governing aerosol optical properties using an ensemble of 1800 aerosol populations from particle-resolved simulations. To balance detailed presentation and computational cost, most chemical transport models typically simplify aerosol representation by tracking separate aerosol populations rather than individual particle components (Riemer et al., 2019). Mie theory based on a simple fixed mixing state (external, fully internal, or core–shell mixing) assumption is often used in chemical transport models (Li et al., 2020; Gao et al., 2020).

Comparison between different mixing states conducted in previous studies showed that BC-absorbing properties are sensitive to mixing state assumptions. Curci et al. (2019) found that aerosol optical depth (AOD) is mainly determined by aerosol mass and only secondarily affected by mixing state; however, absorption enhancement (E_{abs}) values depend on the mixing assumption made in the model. The underestimation of modeled absorption AOD decreased from 66 % in the external mixing case to 43 % in the core–shell mixing case (Tuccella et al., 2020). Partial internal mixing is the most likely mixing state of aerosols. The fraction of internally mixed particles can be calculated using the parameterization of Cheng et al. (2012) and Curci et al. (2019). The fraction of core–shell mixing particles can be parameterized as a function of the bulk volume ratio (Hu et al., 2022). The mixing state index and mass ratio of coating to BC were used to improve the presentation of the BC mixing state, and aerosol particles in the accumulation mode were partitioned into BC-free and BC-containing particles (Shen et al., 2024). E_{abs}, calculated in a partial internal mixing state, was approximately 10 % lower than that from core–shell mixing simulations (Tuccella et al., 2020). However, quantitative investigations considering the evolution of mixing states based on microphysical properties are limited (Li et al., 2024). Therefore, the fraction of coated BC and the coating fraction of other components based on microphysical processes should be considered in the optical calculation.

Coating thickness and the heterogeneity of the mixing state are proposed as the main reasons explaining the gap between field observations, lab investigations, and model simulations in light absorption enhancement (Zhao et al., 2021; Fierce et al., 2020; Wang et al., 2021a). The coating fraction significantly influences the absorption of BC particles. The coating thickness of BC particles can be detected by a single-particle soot photometer (SP2), although the lower measurement limits of SP2 typically result in an overestimation of the concentrations of pure BC (Zhao et al., 2020), and the mass ratio of coating to BC core can highly impact absorption enhancement (Liu et al., 2017; Zhao et al., 2021). The aging process of black carbon is an important source of uncertainty in the assessment of its contribution to global warming (Wang et al., 2022). Black carbon can be coated by other aerosols, which increases the complexity of optical properties. Kang et al. (2023) showed that the aging of BC at night in the residual layer can be higher than in the daytime and can enhance its light absorption. The degree of aging and mixing state can change very quickly in a polluted environment (Peng et al., 2016). An inadequate understanding of the mixing state of BC greatly hinders the assessment of its climate effects (Huang et al., 2023). Due to this complexity, few three-dimensional (3-D) models sufficiently resolve BC aging processes (Xie et al., 2023; Zhang et al., 2019). One

3-D modeling study found that the aging time of BC varied greatly and showed significant spatial heterogeneity over polluted areas in China (Chen et al., 2017b).

In this study, the Nested Air Quality Prediction Modeling System (NAQPMS) coupled with an advanced particle microphysics (APM) module was used to investigate the absorption properties of aerosols over northern China in November 2018. The simulation of aerosol components was conducted using a 3-D air quality model. First, three ideal mixing states (external, internal mixing, and core–shell mixing) were considered to study the effect of the mixing state through the Flexible Aerosol Optical Depth module based on observation and simulation of $PM_{2.5}$ components. Then, the fraction of coated BC based on the degree of aging of BC, the fraction of coating, and detailed microphysical processes were considered during the absorption calculation. Finally, the impact of aging processes on light absorption enhancement was investigated.

2 Data and methods

2.1 Observation data

The study period is from 1 to 30 November 2018. Observations of $PM_{2.5}$ components were obtained from the China National Environmental Monitoring Centre. The observation site in Beijing (BJ), located at the China National Environmental Monitoring Centre (40°2′ N, 116°41′ E), is a typical urban site. Water-soluble species (Na^+, K^+, sulfate, nitrate, ammonium, and Cl^-) in $PM_{2.5}$ were measured by a gas and aerosol collector (GAC), and particles were collected by a wet denuder and detected by ion chromatography. Organic carbon (OC) and elemental carbon (EC) were detected using the thermo-optical transmittance method. OC can further be classified into primary organic carbon (POC) and secondary organic carbon (SOC) using the EC tracer method (Castro et al., 1999; Zhao et al., 2013). A refined EC tracer method is proposed (Zheng et al., 2015; Lin et al., 2009), and data from the lowest 10 % of ambient OC / EC ratios were utilized to estimate the primary OC / EC ratio with the following equations (Fig. S1 in the Supplement).

$$\mathrm{POC} = \mathrm{EC} \times (\mathrm{OC}/\mathrm{EC})_{\mathrm{pri}} + N \quad (1)$$

$$\mathrm{SOC} = \mathrm{OC} - \mathrm{POC} \quad (2)$$

The light extinction parameters were measured at the tower site of the Institute of Atmospheric Physics (IAP), Chinese Academy of Sciences (39°58′28″ N, 116°22′16″ E), Beijing. The absorption coefficient at a wavelength of 880 nm was directly measured by a seven-wavelength Aethalometer (AE33, Aerosol Magee Scientific Corp.) (Sun et al., 2021). A new real-time loading effect compensation algorithm was adopted, which is based on a two-parallel spot measurement of optical absorption (Drinovec et al., 2015). It is worth noting that there may be some uncertainty in the absorption measurement due to the use of the reported multiple-scattering correction factor (Yus-Díez et al., 2021; Qin et al., 2018). The extinction coefficient (b_{ext}, $\lambda = 630$ nm) of $PM_{2.5}$ was measured by a cavity-attenuated phase shift extinction monitor (CAPS PMext Aerodyne Research Inc.). The absorption coefficient at 630 nm was derived using a fitted power law relationship at seven wavelengths (Ran et al., 2016). The absorption coefficient at 880 nm was used to analyze the performance of the model as BC is the major contributor to aerosol absorption at 880 nm. $PM_{2.5}$, components, and absorption data were used to evaluate the model's performance.

2.2 Air quality model

NAQPMS is a 3-D Eulerian terrain-following chemical transport model developed by the Institute of Atmospheric Physics, Chinese Academy of Sciences (Wang et al., 2001). The NAQPMS model, coupled with an advanced particle microphysics (APM) module (Yu and Luo, 2009), was used in this study (Chen et al., 2014). NAQPMS includes physical processes, such as advection, convection, diffusion, and deposition; chemistry processes, such as gas-phase chemistry and aqueous chemistry; and aerosol processes. A volatility basis set (VBS) framework for secondary organic aerosols (SOAs) has been coupled to NAQPMS to improve the representation of SOAs (Yang et al., 2019; Chen et al., 2021). The APM module includes microphysical processes such as nucleation, condensation, evaporation, and coagulation (Yu and Luo, 2009; Chen et al., 2021). Particles are represented by the sectional bin scheme in the APM module. Secondary inorganic particles are distributed by 40 bins covering 0.0012–12 µm. BC and OC are represented using 28 bins, and other primary particles, such as dust and sea salt, are represented by 4 bins. The evolution of particle size distributions and the aging processes of BC due to condensation and coagulation are well reproduced by the model (Chen et al., 2017a; Du et al., 2019).

A two-nested model domain was set up in this study. The parent domain covers northern China at a resolution of 27 km, and the second domain covers Beijing–Tianjin–Hebei and surrounding regions with a resolution of 9 km (see Fig. 1). To represent fine vertical structures, 30 vertical levels were adopted, including 17 levels below 2 km. The Weather Research and Forecasting (WRF) version 4.0.1 mesoscale model was used to provide meteorological fields for NAQPMS. The initial and boundary conditions for meteorology were provided by NCEP final (FNL) reanalysis data every 6 h (https://doi.org/10.5065/D6M043C6, National Centers for Environmental Prediction et al., 2000), and the MOZART model provided initial chemical fields. The Multiresolution Emission Inventory for China (MEIC), developed by Tsinghua University, with a resolution of $0.25 \times 0.25°$ was used (http://meicmodel.org.cn, last access: 4 June 2025). The base year of the emission inventory was 2017. MEIC covers 10 species, including BC, OC, $PM_{2.5}$, PM_{10}, CO, NH_3, SO_2, NO_x, CH_4, and VOCs. The configuration of WRF

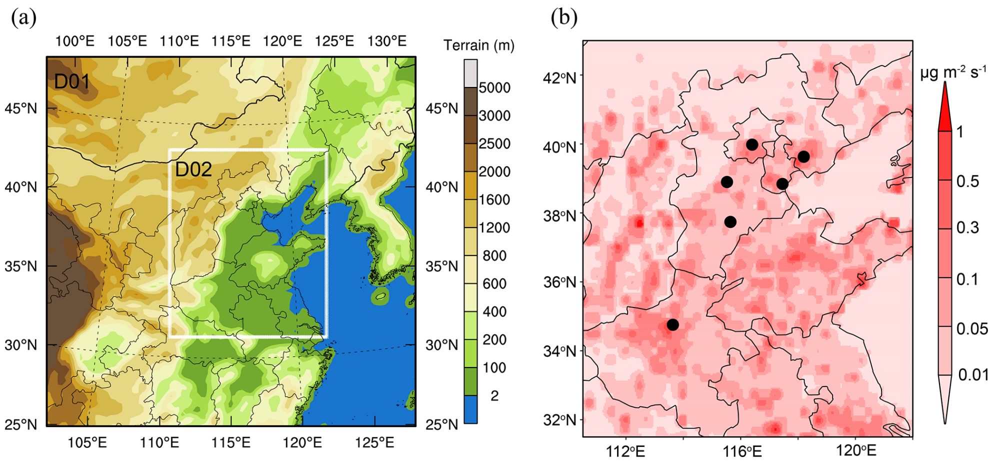

Figure 1. **(a)** The model domain. **(b)** Emission rate of primary $PM_{2.5}$ and the location of observation sites. Black dots are pollution sites.

and NAQPMS can be seen in Table S1. The simulation of WRF and NAQPMS started on 24 October 2018, and the first 7 d was set aside as spin-up time.

2.2.1 Flexible Aerosol Optical Depth (FlexAOD) module

In this study, the particles are assumed to be spherical, and Mie theory (Mie, 1908) is applied to study their optical properties. The FlexAOD module (http://pumpkin.aquila.infn.it/flexaod/, last access: 4 June 2025) (Curci et al., 2015) was employed to calculate extinction and single-scattering albedo. The components of $PM_{2.5}$ and relative humidity (RH) are used as input parameters. The average volume of particles for each species is computed by dividing the mass by the species' density. Mixing states considered in the study include the external mixing (EXT) assumption, the internal homogeneous (HOM) assumption, and the core–shell (CS) assumption. For the external mixing assumption, extinction is the sum of each species under specific relative humidity. For internal mixing cases (HOM and CS), the particles conform to a lognormal size distribution. For the internal homogeneous assumption, the volume average refractive index is a function of particle size applied over all species. For the core–shell assumption, the refractive index for the BC core and homogeneously mixed shell (secondary inorganic aerosols and secondary organic aerosols) is calculated separately. The Mie code based on Toon and Ackerman (1981) is used for the core–shell internal mixing, and the code based on Mishchenko et al. (1999) is adopted for external and homogeneous internal mixing. The size distribution of the different aerosols is taken from the Optical Properties of Aerosols and Clouds (OPAC) database (Hess et al., 1998). The mean diameter of BC is assumed to be 30 nm based on Dentener et al. (2006). The density, complex refractive index, particle hygroscopic growth factor, mean radius, and standard variation in the lognormal size distribution are shown in Table S2.

2.2.2 Optical module based on the APM module

The APM module is a size-resolved and mixing-state-resolved advanced particle microphysics module coupled in NAQPMS. The mixing state in the APM module is assumed to be semi-externally mixed, which includes internal mixing, external mixing, and core–shell mixing. The seeding particles generated by emission and nucleation (including BC, OC, sulfate, dust, and sea salt) can be coated by secondary particles (including sulfate, nitrate, ammonium, and SOA) through condensation, coagulation, chemical reactions, equilibrium uptake, and hygroscopic growth processes. Sulfate coated by secondary inorganic aerosols (SIAs) or SOAs is considered to be internally mixed. BC, OC, dust, and sea salt coated with SIA or SOA are considered to be core–shell mixing. These coated particles are externally mixed. The mixing of BC particles with other aerosol components can be well resolved hourly. More details can be seen in Yu and Luo (2009) and Chen et al. (2017b).

When calculating the optical parameters of aerosols, the scheme by Yu et al. (2012) is used. The particles are assumed to be spherical, and key particle optical properties, including extinction efficiency, single-scattering albedo (SSA), and asymmetry parameters at each wavelength, are calculated by Mie theory based on the core diameter, shell diameter, and real and imaginary components of the refractive index of the core and shell. The core–shell code based on Toon and Ackerman (1981) is used in the APM module. To reduce computation cost, three lookup tables are used: one for particles without solid absorbing cores, the second for coated BC, and the third for coated dust. Volume-averaged refractive indices of species other than BC and dust are calculated based on the composition simulated by NAQPMS. Details can be seen in Yu et al. (2012) and references therein.

2.3 Sensitivity test design

In this study, the 3-D chemical transport model NAQPMS coupled with the advanced particle microphysics (APM) module was used to reproduce the evolution and spatial distribution of pollutants. The mass concentration, size distribution, and mixing state of aerosols are calculated by NAQPMS + APM. FlexAOD is a module that calculates the extinction property of aerosols under different mixing state assumptions based on Mie theory and a fixed size distribution, using the input of aerosol components' mass concentrations and relative humidity, as shown in Sect. 2.2.1. There are two approaches to calculating optical properties. The absorption property of aerosols can be investigated by FlexAOD, with the input of component concentrations simulated by NAQPMS + APM and the assumed size distribution. The fraction of embedded BC and the fraction of coating aerosols calculated by NAQPMS + APM can be used to constrain the mixing state in FlexAOD. In the other approach, the absorption property can be investigated by the optical module based on the APM module, with core and shell information calculated by NAQPMS + APM, as shown in Sect. 2.2.2. Following this, a series of sensitivity tests were designed to explore the impact of the mixing states, components, aging processes, and detailed microphysical processes (Table 1).

First, to examine the effect of the mass concentration and mixing state on the optical properties, sensitivity tests with different mixing states (external, internally homogeneous, and core–shell) were conducted using FlexAOD. EXT_o, HOM_o, and CS_o refer to cases calculated using FlexAOD with observed components as input under external, homogeneous internal, and core–shell mixing states, respectively. EXT_s, HOM_s, and CS_s refer to cases calculated using FlexAOD with components simulated by NAQPMS + APM as input under external, homogeneous internal, and core–shell mixing states, respectively. Comparing EXT_o, HOM_o, and CS_o can reveal the impact of the mixing state, and, similarly, comparing EXT_s, HOM_s, and CS_s further demonstrates this impact. Comparing CS_o with CS_s, the impact of mass concentration on optical properties can be obtained. Second, to investigate the impact of the aging process, simulations were designed using a partial core–shell mixing state in FlexAOD, encompassing two scenarios: CS-F_{in} (all secondary aerosols coating the F_{in} fraction of embedded BC, where fraction refers to mass fraction throughout this study) and CS-$F_{in}F_c$ (F_c fraction of secondary aerosols coating the F_{in} mass fraction of embedded BC), as illustrated in Fig. S2. Additionally, the components, size distribution, and mixing state simulated by NAQPMS + APM were used to calculate the optical properties (CS-APM). The impact of the microphysical processes can be investigated by comparing CS-$F_{in}F_c$ with CS-APM.

2.4 Model evaluation

Statistical parameters, such as the correlation coefficient (R), normalized mean bias (NMB), index of agreement (IOA), fraction of the simulations within a factor of 2 of the observations (FAC2), mean fractional bias (MFB), and mean fractional error (MFE), were used in this study to evaluate the performance of NAQPMS (Table S3). NAQPMS reproduced the temporal distribution of $PM_{2.5}$ in Beijing well (Fig. 2). As shown in Table S4, R between the observed and simulated hourly $PM_{2.5}$ concentrations of six sites over Beijing–Tianjin–Hebei and surrounding regions was within 0.55–0.76. The NMB was within −0.22 to 0.13, which satisfied the model performance criteria proposed by Emery et al. (2017). There was only a small overestimation of 13 % in the simulated $PM_{2.5}$ in Zhengzhou. IOA reached more than 0.72. The MFB and MFE of $PM_{2.5}$ in all six sites were within the benchmarks, which satisfied the model performance criteria proposed by Boylan and Russell (2006).

NAQPMS also exhibited good performance in representing the $PM_{2.5}$ components in Beijing (Fig. 3). The R values between the observed and simulated nitrate, sulfate, ammonium, element carbon, primary organic aerosols, and secondary organic aerosols were 0.74, 0.83, 0.74, 0.55, 0.48, and 0.23 in Beijing, respectively. However, the simulation of secondary inorganic aerosols was underestimated by −62 % to 8 %. This is likely caused by insufficient heterogeneous formation of sulfate and nitrate (Li et al., 2018). Black carbon and primary organic aerosols were overestimated by 7.2 % and 11.5 %, which is probably related to the emission inventory. Monthly mean emissions were used in this study, and there is substantial uncertainty in the emission inventory (Li et al., 2017). However, accurate simulation of aerosol mass concentration provides a solid foundation for simulating the optical properties of BC-containing aerosols.

3 Results

3.1 Absorption properties based on observed components

3.1.1 Description of observations

The time series and proportion of various chemical components of $PM_{2.5}$ are shown in Fig. 4. During the study period, the average mass concentration of $PM_{2.5}$ was $74.4 \pm 68.7\,\mu g\,m^{-3}$. Nitrate was the main component of $PM_{2.5}$, accounting for 36.4 % on average, followed by organic matter, ammonium, and sulfate, accounting for 16.6 %, 15.4 %, and 11.5 %, respectively. EC, crustal elements, and chloride salt accounted for 3.9 %, 8.8 %, and 4.1 %, respectively. The average RH during the period was 39 ± 17.9 %, and the temperature was 8.3 ± 3.2 °C. The average b_{sca} ($\pm 1\sigma$) and b_{abs} ($\pm 1\sigma$) at 630 nm during the study period were 169.1 ± 212.3 and $46.5 \pm 48.5\,Mm^{-1}$ in Beijing, respectively. The average b_{abs} ($\pm 1\sigma$) at 880 nm during the

Table 1. Simulation test design.

Case	Method	Input	Size distribution	Mixing state
EXT_o	FlexAOD	observed	fixed	external
HOM_o	FlexAOD	observed	fixed	internal homogeneous
CS_o	FlexAOD	observed	fixed	core–shell
EXT_s	FlexAOD	simulated	fixed	external
HOM_s	FlexAOD	simulated	fixed	internal homogeneous
CS_s	FlexAOD	simulated	fixed	core–shell
CS-F_{in}	FlexAOD	simulated	fixed	partial core–shell and partial bare BC [a]
CS-$F_{in}F_c$	FlexAOD	simulated	fixed	partial core–shell, partial bare BC, and partial coating aerosols [b]
CS-APM	APM	simulated	simulated	semi-external (hourly) [c]

Impact	Description
EXT_o vs. HOM_o vs. CS_o	impact of mixing state when inputting observed data
EXT_s vs. HOM_s vs. CS_s	impact of mixing state when inputting simulated data
CS_o vs. CS_s	impact of aerosol mass concentration
CS_s vs. CS-F_{in}	impact of aging process (fraction of embedded BC)
CS_s vs. CS-$F_{in}F_c$	impact of the aging process (fraction of embedded BC and coating shell)
CS-$F_{in}F_c$ vs. CS-APM	impact of detailed microphysical process

[a] Aerosols are classified into two types: embedded and bare-like BC aerosols. [b] Aerosols are classified into three types: embedded, bare-like BC, and BC-free aerosols. [c] The concept map can be found in Chen et al. (2019, Fig. 1).

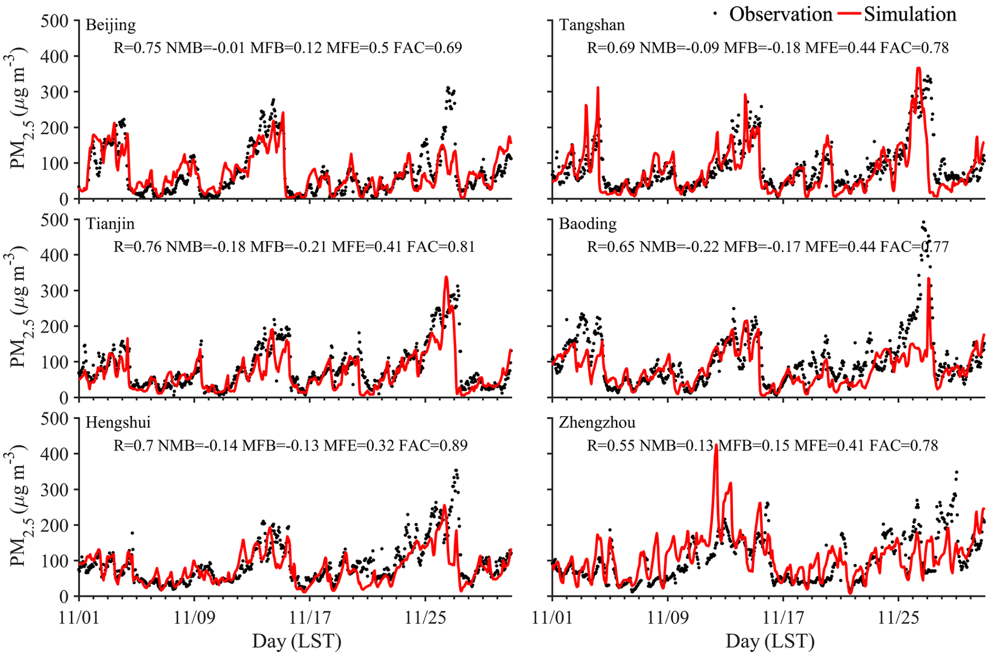

Figure 2. Model evaluation of $PM_{2.5}$ at six sites in the Beijing–Tianjin–Hebei region in November 2018.

study period was $30.7 \pm 25.2\,Mm^{-1}$. b_{abs} at 880 nm and EC mass concentration were highly correlated (Fig. S3). The decrease in visibility is mainly caused by particle scattering extinction. b_{sca} and b_{abs} in this study were much lower than those observed in Beijing in the winter of 2016 (Xie et al., 2019), but b_{ext} in this study was higher than that observed in Beijing in the winter of 2019 (Sun et al., 2021), indicating that the decreases in $PM_{2.5}$ in recent years also caused similar reductions in extinction coefficients.

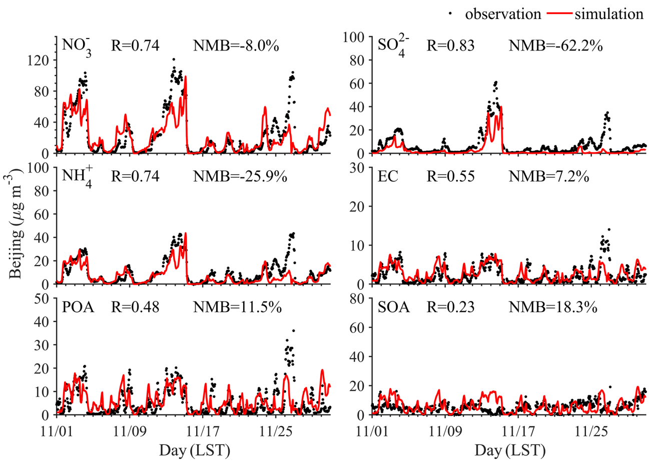

Figure 3. Simulated and observed $PM_{2.5}$ components in Beijing.

3.1.2 Absorption coefficient calculated by FlexAOD based on observations

The observed $PM_{2.5}$ components and RH were used to calculate optical properties using FlexAOD. It should be noted that the periods with missing component data were excluded when calculating optical properties. Comparison between the observed and simulated absorption coefficients shows that the simulations by FlexAOD under the three mixing state assumptions are highly correlated with the observations, and the correlation coefficient can reach 0.88, demonstrating the usability of the FlexAOD model in Beijing. However, using different mixing state assumptions led to widely varying results (see Fig. 5). On average, b_{abs} at 880 nm, calculated for the core–shell mixing state, was 2.4 times higher than that for the external mixing state. For the external mixing state, the calculation was underestimated by 59 %, while it was overestimated by 91 % under uniform internal mixing. The simulation of core–shell mixing was closest to observations, with an underestimation of 2.8 %. The absorption coefficient under uniform internal mixing was the highest, followed by core–shell mixing. The calculation for external mixing was the lowest. This is consistent with the findings of Curci et al. (2019). The assumption of either internal mixing or external mixing alone is not realistic, and partial internal mixing with partial coating closely approximates reality and should be considered for absorption calculations, as reported by Curci et al. (2019).

3.2 Absorption property based on simulations by NAQPMS

A comparison of the absorption coefficients between observations and calculations with FlexAOD based on $PM_{2.5}$ simulations from NAQPMS with different mixing states can be seen in Table 2. In this study, only times in which the simulated $PM_{2.5}$ was within a factor of 2 of the observations were considered in the optical calculation. The average of observed b_{abs} is 43 Mm^{-1}. There were large variations in the absorption coefficient under different mixing states. In the $\mathrm{EXT_s}$ case, the absorption coefficient at 880 nm was underestimated by 54 %, and only 40 % of the modeled values were within a factor of 2 of the observations. In the $\mathrm{HOM_s}$ case, the absorption at 880 nm was largely overestimated by 95 %, with 58 % of the modeled values falling within a factor of 2 of the observations. In the $\mathrm{CS_s}$ case, FAC2 increased to 0.93 compared with $\mathrm{EXT_s}$ simulations, and the model overestimated the absorption coefficient by 10 %. Among the three ideal mixing state assumptions in this study, the result of the core–shell mixing state assumption is closest to the observed absorption coefficient. It should be noted that there are uncertainties associated with the calculation. As shown in Fig. 3, the concentration of secondary inorganic aerosols is underestimated by the NAQPMS model, while BC is overestimated; consequently, the coated thickness may be underestimated. Comparing the results of $\mathrm{CS_s}$ with $\mathrm{CS_o}$ (where calculations with FlexAOD were based on observed components under a core–shell mixing state) shows that the effect of simulated components on the absorption coefficient can be up to 13 %, which is much smaller than the impact of the mixing state.

Table 2. Intercomparison of the performance of absorption coefficients at 880 nm under different mixing states, where b is the ratio of simulations to observations.

Schemes	b	R	NMB	FAC2
$\mathrm{EXT_s}$	0.46	0.82	−0.54	0.40
$\mathrm{HOM_s}$	1.95	0.79	0.95	0.58
$\mathrm{CS_s}$	1.10	0.82	0.10	0.93
CS-F_{in}	0.83	0.77	−0.17	0.84
CS-$F_{\mathrm{in}}F_{\mathrm{c}}$	0.66	0.78	−0.34	0.66
CS-APM	0.58	0.79	−0.42	0.72

3.3 Constraint of the fraction of embedded BC and secondary component coating on aerosols

In the real world, the mixing state of particles is complex. Using an electron microscope, Wang et al. (2021b) found that the embedded fraction of BC significantly influenced the absorption. In the extremely polluted winter period of January 2013, more than half of BC particles were thickly coated by non-refractory materials (Wu et al., 2016). With the implementation of the Air Pollution Prevention and Control Action Plan, the mass of BC and the fraction of thickly coated BC changed (Wu et al., 2021). Cheng et al. (2012) proposed that the fraction of internally mixed particles can be parameterized based on oxidized nitrogen oxides and total reactive nitrogen. Curci et al. (2019) used the mass ratio of secondary inorganic aerosols and organics to BC as the fraction of internally mixed particles.

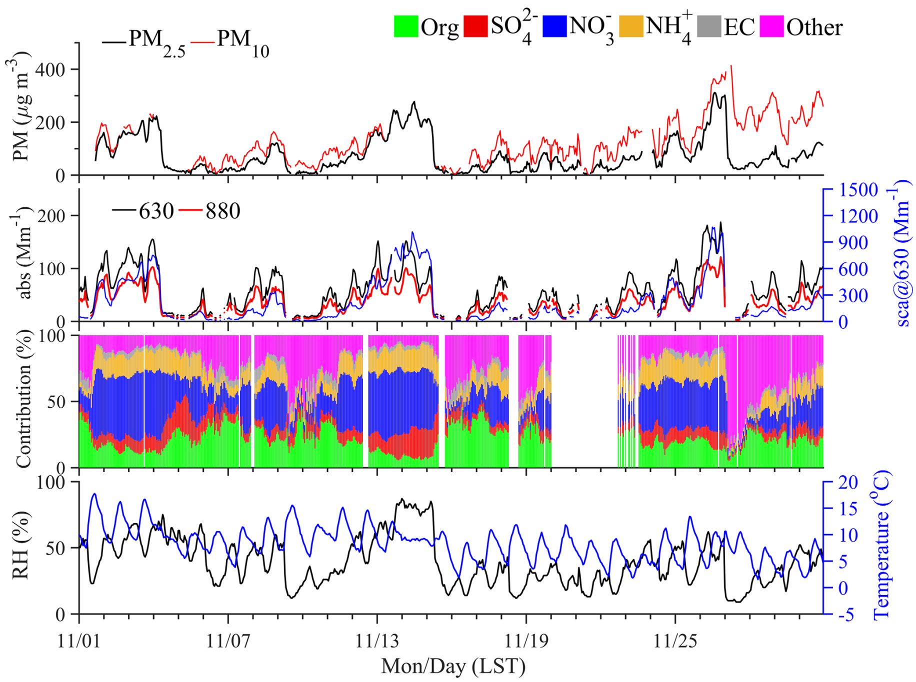

Figure 4. Evolution of observed $PM_{2.5}$, components, aerosol extinction coefficient, and meteorology parameters in November 2018 in Beijing.

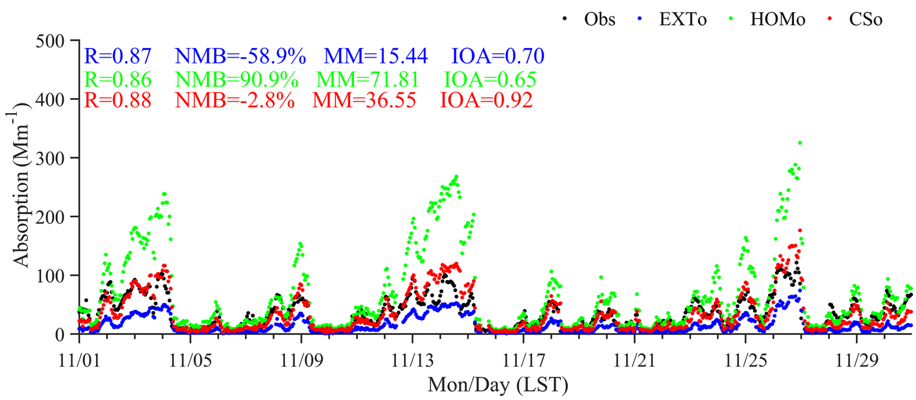

Figure 5. Observed and calculated absorption coefficients at 880 nm under external mixing (EXT_o), homogeneous internal mixing (HOM_o), and core–shell mixing (CS_o) by FlexAOD based on observed components.

Emitted hydrophobic black carbon becomes hydrophilic due to aging processes. In this study, the aging of BC can be resolved by NAQPMS + APM. Detailed aging processes of aerosols are considered in a physical manner. The model represents the aging processes by simulating condensation and coagulation. The ratio of hydrophilic BC to total BC is used as a proxy for the fraction of embedded BC. The evolution of the ratio of particle diameter to BC core size (D_p/D_c), the fraction of embedded BC (F_{in}), and the fraction of secondary component coating on BC (F_c) at the site in Beijing are shown in Fig. 7. When F_{in} is equal to 0, it means the BC is externally mixed with other aerosols, and when F_{in} is equal to 1, it means all BC particles are coated by other aerosols. The average ratio of F_{in} during the study period in Beijing is 34.1 %, which is slightly lower than the ratio of 0.48 and 0.63 obtained by the method of Cheng et al. (2012) and Curci et al. (2019), respectively. Moreover, F_{in} in this study is closely related to the ratio of secondary inorganic aerosols to BC, with an R of 0.72. Zheng et al. (2022) also found with online observational datasets that secondary inorganic aerosols dominated light absorption enhancement. We consider a separate case, CS-F_{in}, where the F_{in} mass fraction of BC particles is core–shell mixed with other aerosols, and the $1 - F_{in}$ fraction of BC particles consists of bare and external mixing. The calculated absorption at 880 nm (b_{abs_880}) for the CS-F_{in} case was 35.5 Mm^{-1}, which was close to the measured mean value, and 84 % of simulations of absorption coefficients were within a factor of 2 of the observations.

Aerosols in the atmosphere include BC-containing aerosols (coated BC and bare BC) and BC-free aerosols (Zhao et al., 2022). In this study, the fraction of secondary aerosol coating on BC is also considered in the optical calculation. As sulfate aerosols include sulfate coating on BC, OC, dust, and sea salts, the fraction of sulfate coating on BC was thus used as the fraction of secondary component coating on BC (F_c). When F_c is equal to 0, there is no coating on BC particles, and when F_c is equal to 1, it means all other aerosols are coated on BC. We thus consider a scenario CS-$F_{in}F_c$, where the F_{in} fraction of BC particles and the F_c fraction of secondary components are core–shell mixed, and other aerosols are externally mixed. The average F_c during the study period in Beijing is 34.3 %. The calculated absorption at 880 nm for the CS-$F_{in}F_c$ case was 28.1 Mm^{-1}, and 66 % of the simulations of absorption coefficients were within a factor of 2 of the observations.

As described in Sect. 2.2.2, optical properties were calculated based on Mie theory using the core and shell information derived from the APM module considering microphysical processes. The observed absorption coefficient and that simulated by NAQPMS + APM under a semi-external mixing state, namely CS-APM, are shown in Table 2 and Fig. 6f. The results show that the simulated absorption at 880 nm matches the observation reasonably well, with an R of 0.79, although there is an underestimation with an NMB of 0.42. The CS-$F_{in}F_c$ case considers the fraction of embedded BC and the fraction of secondary component coating BC calculated with the APM module. Comparison between CS-$F_{in}F_c$ and CS-APM reveals the impact of accounting for detailed microphysical processes on absorption property. The FAC2 of 0.72 in the CS-APM case is greater than 0.66 in the CS-$F_{in}F_c$ case. The underestimation of 42 % in CS-APM is larger than the 34 % underestimation in CS-$F_{in}F_c$. This underestimation can be attributed to the assumed morphology of BC-containing particles, the size distribution of primary particles input to the APM module, and the concentration of secondary components coated on BC. As shown in Fig. 3, there is an underestimation of 8 %–62 % in the simulation of secondary inorganic aerosols. Even if the model accurately captures the physical processes of aerosols, the coating on BC could be underestimated because of the representation uncertainties in chemical formation, potentially impacting the accuracy of the absorption calculation.

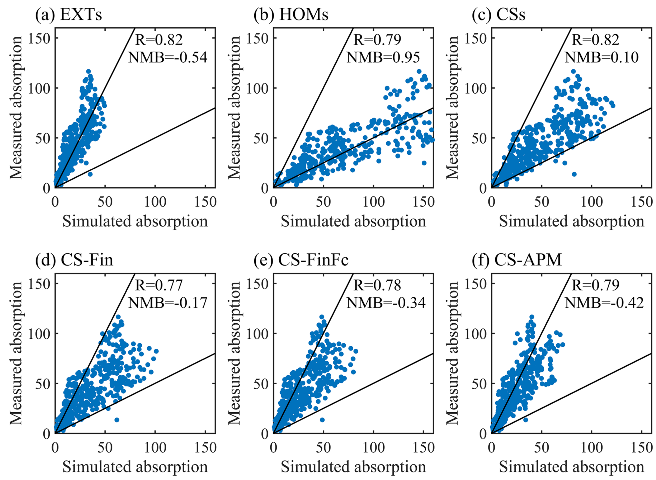

Figure 6. Comparison of observed and simulated absorption coefficients at 880 nm under different mixing states (EXT_s, HOM_s, CS_s, CS-F_{in}, CS-$F_{in}F_c$, and CS-APM) at the IAP in Beijing.

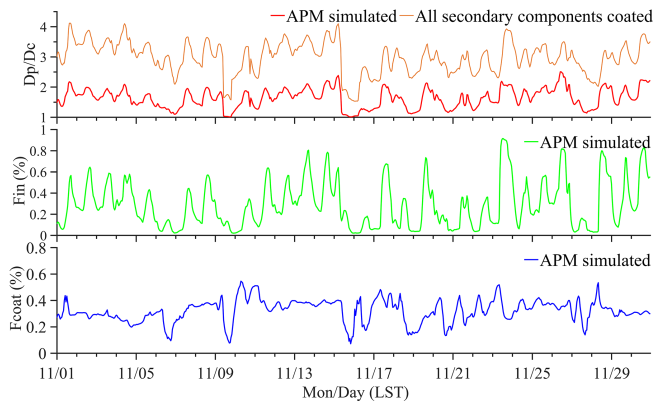

Figure 7. Evolution of the ratio of particle diameter to BC core size (D_p/D_c), the fraction of embedded BC (F_{in}), and the fraction of secondary component coating on BC (F_c) at IAP in Beijing. "APM simulated" refers to parameters simulated by the advanced particle microphysics module in NAQPMS.

3.4 Light absorption enhancement due to mixing state and aging processes

The light absorption enhancement is the ratio of the light absorption coefficient of coated BC and bare BC. E_{abs} is proposed to quantify the lensing effects; however, large uncertainty exists in E_{abs} and the radiative effect of black carbon. In this study, the BC absorption enhancement is calculated as the ratio of the absorption coefficient calculated assuming core–shell mixing (including CS_s, CS-F_{in}, and CS-$F_{in}F_c$ cases) to that calculated using external mixing.

$$E_{abs} = \frac{b_{abs}(\lambda, \text{core–shell mixing})}{b_{abs}(\lambda, \text{external mixing})} \tag{3}$$

3.4.1 The impact of detailed microphysical processes on absorption enhancement

We modified the APM module in NAQPMS so that BC does not mix with other chemical species in the calculation of the microphysical processes and optical properties. This sensitivity test was conducted by turning off the coating process in the APM module. The radiative absorption enhancement

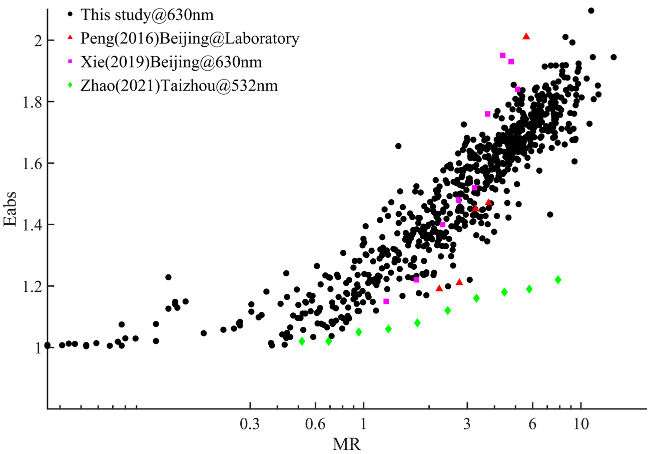

Figure 8. The absorption enhancement in the CS-APM case under different mass ratios (MRs) of coating materials and the BC core.

in the CS-APM case was the ratio of the absorption coefficient in the base simulation to that in the sensitivity test.

The mass ratio of the coating of BC to BC (MR) can be used to represent the degree of aging (Du et al., 2019; Wang et al., 2019). To compare with previous studies, E_{abs} values at 630 nm are shown in Fig. 8. The evolution of E_{abs} and MR shows that E_{abs} is positively correlated to MR, and R can reach 0.88. This is consistent with Liu et al. (2017), who showed that E_{abs} is closely related to MR. Under the same MR, E_{abs} can vary by 0.49. When MR equals 3, E_{abs} varies by 0.25. E_{abs} in the CS-APM case in Beijing is much higher than the measurements in Taizhou (Zhao et al., 2021). However, the measurements in Beijing by Xie et al. (2019) fall in the range of this study when MR is less than 5. E_{abs} in the CS-APM case is higher than that from the laboratory study in Peng et al. (2016) when MR is less than 3, but it is lower when MR exceeds 5.

The spatial distribution of E_{abs} at 880 nm (E_{abs_880}) is shown in Fig. 9d. E_{abs_880} over Beijing–Tianjin–Hebei and the surrounding region is about 1.3–1.8. E_{abs_880} in the CS-APM case is slightly higher than that in the CS-$F_{in}F_c$ case. The spatial distribution of E_{abs_880} also shows lower values of 1.3–1.7 over the source region and higher values of 1.6–1.8 over the outflow region. The average E_{abs} values in Beijing at 630 and 880 nm from the APM module and Mie theory are 1.58 and 1.55.

3.4.2 Impact of aging processes on light absorption enhancement

The spatial distribution of E_{abs} at 880 nm is shown in Fig. 9. The spatial distribution of the absorption enhancement in the CS-F_{in} and CS-$F_{in}F_c$ cases shows that E_{abs} is lower near the emission source and higher in the outflow region (Bohai and Yellow seas, Taihang Mountains). This is because BC has aged through condensation and coagulation processes during transport in the atmosphere. As shown in the figure, the values of E_{abs_880} over Beijing–Tianjin–Hebei and the surrounding region from FlexAOD under the core–shell mixing state are about 2.0–2.5. After considering the fraction of embedded BC, E_{abs} decreases to 1.3–2.1, representing a decrease of 11 %–34 %. Considering the fraction of embedded BC and the fraction of coating, E_{abs} decreases to 1.2–1.7, representing a decrease of 30 %–43 %. The values of E_{abs} in the CS-$F_{in}F_c$ case are 1.2–1.5 near the emission sources and 1.5–1.7 over the outflow region. These values are similar to the currently accepted range of 1.2–1.6 (Bond et al., 2013; Matsui et al., 2016; Liu et al., 2017; Curci et al., 2019). The distribution of average E_{abs} and SSA values with height in Beijing is shown in Fig. 10. In the CS-F_{in} and CS-$F_{in}F_c$ cases, E_{abs} increases with height, while SSA decreases with height. Relatively low E_{abs} values (1.3–1.6) are concentrated in layers below 500 m. This is related to the low level of anthropogenic emissions and to the ability of BC in the upper layer to be transported over wider regions.

In Beijing, the absorption enhancement at 630 and 880 nm is 2.65 and 2.39 for the core–shell mixing state using FlexAOD (Fig. 11). When considering the fraction of embedded BC, the E_{abs} values in the CS-F_{in} case at 630 and 880 nm are 1.94 and 1.80, decreasing by 26.7 % and 24.5 % compared to the CS case, respectively. If the fraction of secondary aerosol coating on BC is also considered at the same time, the E_{abs} values in the CS-$F_{in}F_c$ case at 630 and 880 nm are 1.51 and 1.43, decreasing by 43 % and 40.2 % compared to the CS case, respectively. Therefore, considering the fraction of secondary aerosol coating on BC, E_{abs} at 630 and 880 nm can decrease by 16.2 % and 15.7 %, respectively, compared to the CS case. The ratios of E_{abs} at 880 to E_{abs} at 630 nm under different mixing states in this study were consistently less than 1. This is consistent with the fact that E_{abs} is expected to decrease with increasing wavelengths (Liu et al., 2018).

Comparing the E_{abs} values obtained in this study under different mixing states with those obtained in previous studies, E_{abs} in the CS-F_{in} and CS-$F_{in}F_c$ cases with respect to the aging process were slightly higher than those in other laboratory and ambient measurement studies in Beijing (1.03–1.3) (Wang et al., 2019). Sun et al. (2021), using the thermodenuder (TD) method, found that E_{abs} at 870 nm at an urban site in Beijing was 1.24 ± 0.15. Zhang et al. (2021), using the mass absorption cross-section (MAC) method through SP2, found that E_{abs} at 880 nm at a rural site in Gucheng was 1.33 ± 0.57. Cui et al. (2016) found that E_{abs} increased from 1.4 during fresh combustion to approximately 3 for aged BC at a rural site on the North China Plain. However, the results for the CS-F_{in}, CS-$F_{in}F_{c,}$, and CS-APM cases were lower than those in other model simulations (Curci et al., 2019; Tuccella et al., 2020). The results show that accounting for the aging process of BC has a significant effect on the absorption enhancement and should be considered during model E_{abs} calculation.

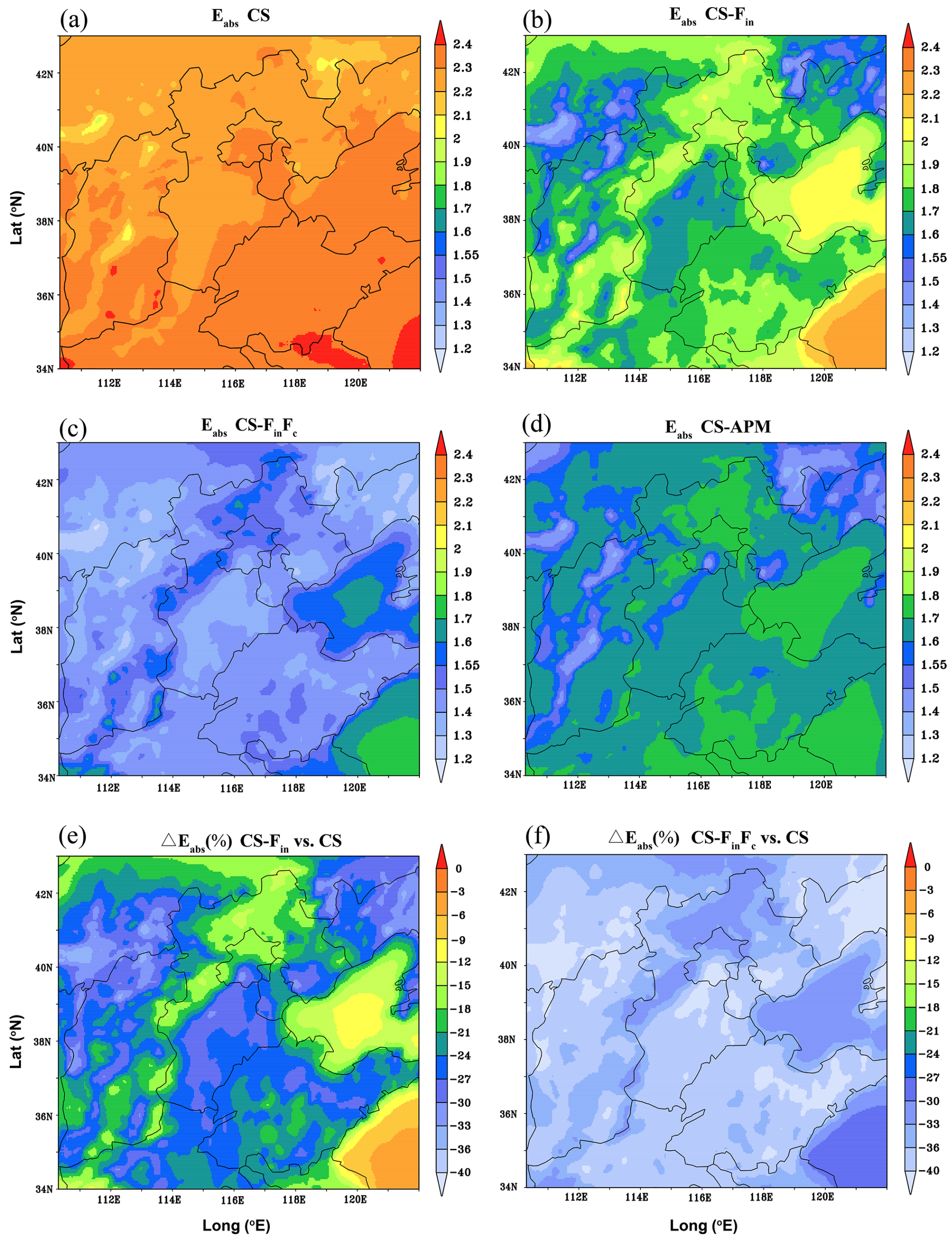

Figure 9. The absorption enhancement at 880 nm in the **(a)** core–shell (CS) mixing, **(b)** CS-F_{in}, **(c)** CS-$F_{\mathrm{in}}F_{\mathrm{c}}$, and **(d)** CS-APM cases. Changes in radiation absorption enhancement in the **(e)** CS-F_{in} and **(f)** CS-$F_{\mathrm{in}}F_{\mathrm{c}}$ cases compared with the core–shell mixing case.

4 Conclusions and discussion

Black-carbon-containing aerosols have a significant impact on global warming. However, the extent of the impacts is highly uncertain. Component concentration, mixing state, and aging processes are important parameters. In this study, observed and simulated concentrations of $PM_{2.5}$ components in November 2018 are used with Mie theory to investigate the impact of the mixing state and aging process on the light absorption properties of aerosols.

Through a series of sensitivity tests, a systematic comparison was conducted to explore the impacts of components, mixing states, aging processes, and detailed microphysics on absorption properties. Under the same mixing state with observed and simulated components, b_{abs} can be highly impacted by the simulated concentration of $PM_{2.5}$ components. Sensitivity tests with different mixing states (external, internally homogeneous, and core–shell) using FlexAOD showed that different mixing state assumptions led to widely varying

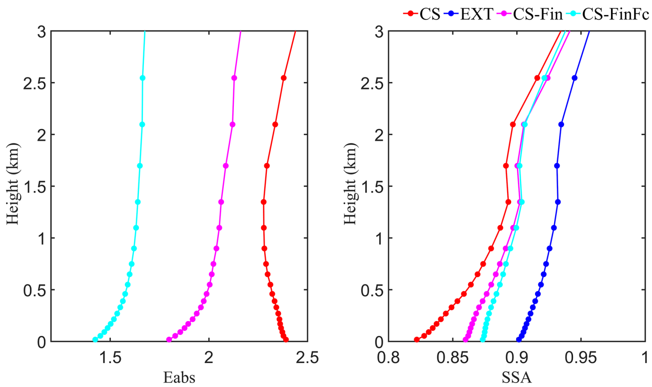

Figure 10. The distribution of E_{abs} and SSA values with height.

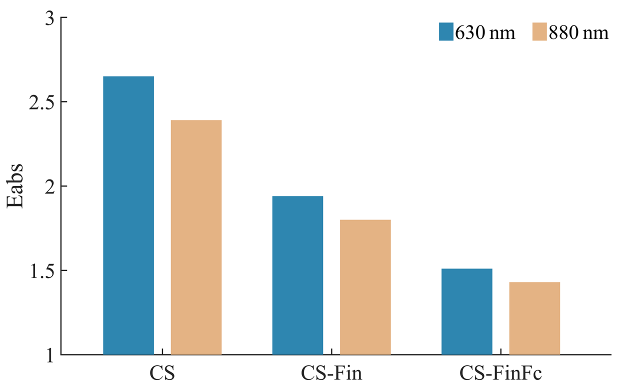

Figure 11. The radiation absorption enhancement at 630 and 880 nm under different mixing state assumptions in Beijing.

results. The absorption coefficient is the highest under uniform internal mixing, lower under core–shell mixing (which is closest to observations), and the lowest under external mixing.

Considering the fraction of embedded BC and secondary component coating on BC is a compromise and a reasonable solution for representing the mixing state of BC in a 3-D model, although uncertainties exist. The detailed microphysical processes can be resolved by an advanced particle microphysics module in NAQPMS. The ratio of hydrophilic BC to total BC is used as a proxy for the fraction of embedded BC, and the fraction of sulfate coating on BC is used as a proxy for the fraction of secondary component coating on BC. Following this, the fraction of embedded BC and secondary component coating on aerosols was used to constrain the mixing state. The simulation of absorption is also reasonable when considering the fraction of embedded BC and coating of secondary components on BC, as this reflects a more realistic mixing state. The NMB of the simulated absorption coefficient changed from 10 % to −34 % in Beijing, and R changed from 0.82 to 0.78.

Accounting for the aging process of BC has a significant effect on radiative absorption enhancement. E_{abs} at 880 nm over the Beijing–Tianjin–Hebei area reduced from 2.0–2.5 under the core–shell mixing state to 1.3–2.1 when considering the fraction of embedded BC and to 1.2–1.7, a decrease of 30 %–42 %, when considering the fraction of embedded BC and the fraction of coating. Considering the detailed microphysical processes, E_{abs} in the CS-APM case was positively correlated with MR with an R of 0.88. The E_{abs} values in the CS-$F_{in}F_c$ and CS-APM cases were slightly higher than those from other laboratory and ambient measurement studies in Beijing but were within the range of previous studies.

The optical properties can be affected by uncertainties in the size distribution of primary particle emissions (Zhou et al., 2012; Matsui, 2016). Geometric radius and standard variation are two important parameters of size distribution. The optical depth of mineral dust and organic carbon was sensitive to standard variation (Obiso and Jorba, 2018). There is a sectoral and spatial difference in the size distribution of primary emissions (Paasonen et al., 2016). Sensitivity tests should be conducted to see the impact of size distribution on σ_{abs} and E_{abs} in future studies. More efforts considering the morphology and the absorption characteristics of coating can also help understand the radiative effect of BC-containing aerosols (Liu et al., 2020; Li et al., 2024).

Overall, this study underscores the importance of representing microphysical processes related to BC aerosols and their mixing state. Our results indicate that resolving the fraction of coated BC and the coating layer can significantly impact the calculated E_{abs}. Although modeling the mixing state and microphysical processes is challenging for the chemical transport model in this study, the fraction of aged BC and coating aerosols can be used to constrain the mixing state. This study provides a reference for simulating the radiative effect of black carbon aerosols using 3-D models.

Code and data availability. The NCEP final (FNL) reanalysis data for WRF are available from https://doi.org/10.5065/D6M043C6 (National Centers for Environmental Prediction et al., 2000). The $PM_{2.5}$ observation data can be obtained from the China National Environmental Monitoring Centre (https://air.cnemc.cn:18007/ (CNEMC, 2025). The FlexAOD code can be provided upon request to gabriele.curci@aquila.infn.it (https://pumpkin.aquila.infn.it/flexaod/, last access: 4 June 2025). The simulated data of this study are available upon request to the corresponding author.

Supplement. The supplement related to this article is available online at https://doi.org/10.5194/acp-25-5665-2025-supplement.

Author contributions. HD, JL, and XC designed the work. HD performed the simulation and analysis. GC and ZFW provided the software. YS, XD, and SG processed the measurement data. ZW, WY, and LW validated the simulated data. HD wrote the original draft with assistance from all co-authors. JL, XC, and FY reviewed and edited the paper.

Competing interests. At least one of the (co-)authors is a member of the editorial board of *Atmospheric Chemistry and Physics*. The peer-review process was guided by an independent editor, and the authors also have no other competing interests to declare.

Disclaimer. Publisher's note: Copernicus Publications remains neutral with regard to jurisdictional claims made in the text, published maps, institutional affiliations, or any other geographical representation in this paper. While Copernicus Publications makes every effort to include appropriate place names, the final responsibility lies with the authors.

Acknowledgements. We thank the technical support of the National Large Scientific and Technological Infrastructure "Earth System Numerical Simulation Facility" (https://cstr.cn/31134.02.EL, last access: 4 June 2025).

Financial support. This research has been supported by the Strategic Priority Research Program of the Chinese Academy of Sciences (grant no. XDB0760302), the National Key Research and Development Program of China (grant no. 2022YFC3700703), the National Natural Science Foundation of China (grant nos. 42207133, 42377105, and 42122049), and the Inner Mongolia Key Research and Development Plan (grant no. 2022YFHH0116).

Review statement. This paper was edited by Birgit Wehner and reviewed by three anonymous referees.

References

Bond, T. C., Doherty, S. J., Fahey, D. W., Forster, P. M., Berntsen, T., DeAngelo, B. J., Flanner, M. G., Ghan, S., Karcher, B., Koch, D., Kinne, S., Kondo, Y., Quinn, P. K., Sarofim, M. C., Schultz, M. G., Schulz, M., Venkataraman, C., Zhang, H., Zhang, S., Bellouin, N., Guttikunda, S. K., Hopke, P. K., Jacobson, M. Z., Kaiser, J. W., Klimont, Z., Lohmann, U., Schwarz, J. P., Shindell, D., Storelvmo, T., Warren, S. G., and Zender, C. S.: Bounding the role of black carbon in the climate system: A scientific assessment, J. Geophys. Res.-Atmos., 118, 5380–5552, https://doi.org/10.1002/jgrd.50171, 2013.

Bondy, A. L., Bonanno, D., Moffet, R. C., Wang, B., Laskin, A., and Ault, A. P.: The diverse chemical mixing state of aerosol particles in the southeastern United States, Atmos. Chem. Phys., 18, 12595–12612, https://doi.org/10.5194/acp-18-12595-2018, 2018.

Boylan, J. W. and Russell, A. G.: PM and light extinction model performance metrics, goals, and criteria for three-dimensional air quality models, Atmos. Environ., 40, 4946–4959, https://doi.org/10.1016/j.atmosenv.2005.09.087, 2006.

Castro, L., Pio, C., Harrison, R., and Smith, D.: Carbonaceous Aerosol in Urban and Rural European Atmospheres: Estimation of Secondary Organic Carbon Concentrations, Atmos. Environ., 33, 2771–2781, https://doi.org/10.1016/s1352-2310(98)00331-8, 1999.

Chen, X. S., Wang, Z. F., Li, J., and Yu, F. Q.: Development of a Regional Chemical Transport Model with Size-Resolved Aerosol Microphysics and Its Application on Aerosol Number Concentration Simulation over China, SOLA, 10, 83–87, https://doi.org/10.2151/sola.2014-017, 2014.

Chen, X., Wang, Z., Li, J., Chen, H., Hu, M., Yang, W., Wang, Z., Ge, B., and Wang, D.: Explaining the spatiotemporal variation of fine particle number concentrations over Beijing and surrounding areas in an air quality model with aerosol microphysics, Environ. Pollut., 231, 1302–1313, https://doi.org/10.1016/j.envpol.2017.08.103, 2017a.

Chen, X. S., Wang, Z. F., Yu, F. Q., Pan, X. L., Li, J., Ge, B. Z., Wang, Z., Hu, M., Yang, W. Y., and Chen, H. S.: Estimation of atmospheric aging time of black carbon particles in the polluted atmosphere over central-eastern China using microphysical process analysis in regional chemical transport model, Atmos. Environ., 163, 44–56, https://doi.org/10.1016/j.atmosenv.2017.05.016, 2017b.

Chen, X., Yang, W., Wang, Z., Li, J., Hu, M., An, J., Wu, Q., Wang, Z., Chen, H., Wei, Y., Du, H., and Wang, D.: Improving new particle formation simulation by coupling a volatility-basis set (VBS) organic aerosol module in NAQPMS + APM, Atmos. Environ., 204, 1–11, https://doi.org/10.1016/j.atmosenv.2019.01.053, 2019.

Chen, X., Yu, F., Yang, W., Sun, Y., Chen, H., Du, W., Zhao, J., Wei, Y., Wei, L., Du, H., Wang, Z., Wu, Q., Li, J., An, J., and Wang, Z.: Global–regional nested simulation of particle number concentration by combing microphysical processes with an evolving organic aerosol module, Atmos. Chem. Phys., 21, 9343–9366, https://doi.org/10.5194/acp-21-9343-2021, 2021.

Chen, X., Ye, C., Wang, Y., Wu, Z., Zhu, T., Zhang, F., Ding, X., Shi, Z., Zheng, Z., and Li, W.: Quantifying evolution of soot mixing state from transboundary transport of biomass burning emissions, iScience, 26, 108125, https://doi.org/10.1016/j.isci.2023.108125, 2023.

Cheng, Y. F., Su, H., Rose, D., Gunthe, S. S., Berghof, M., Wehner, B., Achtert, P., Nowak, A., Takegawa, N., Kondo, Y., Shiraiwa, M., Gong, Y. G., Shao, M., Hu, M., Zhu, T., Zhang, Y. H., Carmichael, G. R., Wiedensohler, A., Andreae, M. O., and Pöschl, U.: Size-resolved measurement of the mixing state of soot in the megacity Beijing, China: diurnal cycle, aging and parameterization, Atmos. Chem. Phys., 12, 4477–4491, https://doi.org/10.5194/acp-12-4477-2012, 2012.

China National Environmental Monitoring Center (CNEMC): National Urban Air Quality Real-time Data Release Platform, China National Environmental Monitoring Center [data set], https://air.cnemc.cn:18007/, last access: 4 June 2025.

Cui, X. J., Wang, X. F., Yang, L. X., Chen, B., Chen, J. M., Andersson, A., and Gustafsson, O.: Radiative absorption enhancement from coatings on black carbon aerosols, Sci. Total Environ., 551, 51–56, https://doi.org/10.1016/j.scitotenv.2016.02.026, 2016.

Curci, G., Hogrefe, C., Bianconi, R., Im, U., Balzarini, A., Baró, R., Brunner, D., Forkel, R., Giordano, L., Hirtl, M., Honzak, L., Jiménez-Guerrero, P., Knote, C., Langer, M., Makar, P. A., Pirovano, G., Pérez, J. L., San José, R., Syrakov, D., Tuccella, P., Werhahn, J., Wolke, R., Žabkar, R., Zhang, J., and Galmarini, S.: Uncertainties of simulated aerosol optical properties induced by assumptions on aerosol physical and chemical properties: An AQMEII-2 perspective, Atmos. Environ., 115, 541–552, https://doi.org/10.1016/j.atmosenv.2014.09.009, 2015.

Curci, G., Alyuz, U., Barò, R., Bianconi, R., Bieser, J., Christensen, J. H., Colette, A., Farrow, A., Francis, X., Jiménez-Guerrero, P., Im, U., Liu, P., Manders, A., Palacios-Peña, L., Prank, M., Pozzoli, L., Sokhi, R., Solazzo, E., Tuccella, P., Unal, A., Vivanco, M. G., Hogrefe, C., and Galmarini, S.: Modelling black carbon absorption of solar radiation: combining external and internal mixing assumptions, Atmos. Chem. Phys., 19, 181–204, https://doi.org/10.5194/acp-19-181-2019, 2019.

Curtis, J. H., Riemer, N., and West, M.: A single-column particle-resolved model for simulating the vertical distribution of aerosol mixing state: WRF-PartMC-MOSAIC-SCM v1.0, Geosci. Model Dev., 10, 4057–4079, https://doi.org/10.5194/gmd-10-4057-2017, 2017.

Dentener, F., Kinne, S., Bond, T., Boucher, O., Cofala, J., Generoso, S., Ginoux, P., Gong, S., Hoelzemann, J. J., Ito, A., Marelli, L., Penner, J. E., Putaud, J.-P., Textor, C., Schulz, M., van der Werf, G. R., and Wilson, J.: Emissions of primary aerosol and precursor gases in the years 2000 and 1750 prescribed data-sets for AeroCom, Atmos. Chem. Phys., 6, 4321–4344, https://doi.org/10.5194/acp-6-4321-2006, 2006.

Drinovec, L., Močnik, G., Zotter, P., Prévôt, A. S. H., Ruckstuhl, C., Coz, E., Rupakheti, M., Sciare, J., Müller, T., Wiedensohler, A., and Hansen, A. D. A.: The "dual-spot" Aethalometer: an improved measurement of aerosol black carbon with real-time loading compensation, Atmos. Meas. Tech., 8, 1965–1979, https://doi.org/10.5194/amt-8-1965-2015, 2015.

Du, H., Li, J., Chen, X., Wang, Z., Sun, Y., Fu, P., Li, J., Gao, J., and Wei, Y.: Modeling of aerosol property evolution during winter haze episodes over a megacity cluster in northern China: roles of regional transport and heterogeneous reactions of SO_2, Atmos. Chem. Phys., 19, 9351–9370, https://doi.org/10.5194/acp-19-9351-2019, 2019.

Emery, C., Liu, Z., Russell, A., Odman, M., Yarwood, G., and Kumar, N.: Recommendations on Statistics and Benchmarks to Assess Photochemical Model Performance, J. Air Waste Manage., 67, 582–598, https://doi.org/10.1080/10962247.2016.1265027, 2017.

Fierce, L., Riemer, N., and Bond, T. C.: Toward Reduced Representation of Mixing State for Simulating Aerosol Effects on Climate, B. Am. Meteorol. Soc., 98, 971–980, https://doi.org/10.1175/bams-d-16-0028.1, 2017.

Fierce, L., Onasch, T. B., Cappa, C. D., Mazzoleni, C., China, S., Bhandari, J., Davidovits, P., Fischer, D. A., Helgestad, T., Lambe, A. T., Sedlacek, A. J., 3rd, Smith, G. D., and Wolff, L.: Radiative absorption enhancements by black carbon controlled by particle-to-particle heterogeneity in composition, P. Natl. Acad. Sci. USA, 117, 5196–5203, https://doi.org/10.1073/pnas.1919723117, 2020.

Fuller, K. A., Malm, W. C., and Kreidenweis, S. M.: Effects of mixing on extinction by carbonaceous particles, J. Geophys. Res.-Atmos., 104, 15941–15954, https://doi.org/10.1029/1998jd100069, 1999.

Gao, M., Han, Z., Tao, Z., Li, J., Kang, J.-E., Huang, K., Dong, X., Zhuang, B., Li, S., Ge, B., Wu, Q., Lee, H.-J., Kim, C.-H., Fu, J. S., Wang, T., Chin, M., Li, M., Woo, J.-H., Zhang, Q., Cheng, Y., Wang, Z., and Carmichael, G. R.: Air quality and climate change, Topic 3 of the Model Inter-Comparison Study for Asia Phase III (MICS-Asia III) – Part 2: aerosol radiative effects and aerosol feedbacks, Atmos. Chem. Phys., 20, 1147–1161, https://doi.org/10.5194/acp-20-1147-2020, 2020.

Hess, M., Koepke, P., and Schult, I.: Optical properties of aerosols and clouds: The software package OPAC, B. Am. Meteorol. Soc., 79, 831–844, https://doi.org/10.1175/1520-0477(1998)079<0831:Opoaac>2.0.Co;2, 1998.

Hu, K., Liu, D., Tian, P., Wu, Y., Li, S., Zhao, D., Li, R., Sheng, J., Huang, M., Ding, D., Liu, Q., Jiang, X., Li, Q., and Tao, J.: Identifying the Fraction of Core–Shell Black Carbon Particles in a Complex Mixture to Constrain the Absorption Enhancement by Coatings, Environ. Sci. Tech. Let., 9, 272–279, https://doi.org/10.1021/acs.estlett.2c00060, 2022.

Huang, X.-F., Peng, Y., Wei, J., Peng, J., Lin, X.-Y., Tang, M.-X., Cheng, Y., Men, Z., Fang, T., Zhang, J., He, L.-Y., Cao, L.-M., Liu, C., Zhang, C., Mao, H., Seinfeld, J. H., and Wang, Y.: Microphysical complexity of black carbon particles restricts their warming potential, One Earth, 7, 136–145, https://doi.org/10.1016/j.oneear.2023.12.004, 2023.

IPCC: Climate Change 2021: The Physical Science Basis. Contribution of Working Group I to the Sixth Assessment Report of the Intergovernmental Panel on Climate Change, edited by: Masson-Delmotte, V., Zhai, P., Pirani, A., Connors, S. L., Péan, C., Berger, S., Caud, N., Chen, Y., Goldfarb, L., Gomis, M. I., Huang, M., Leitzell, K., Lonnoy, E., Matthews, J. B. R., Maycock, T. K., Waterfield, T., Yelekçi, O., Yu, R., and Zhou, B., Cambridge University Press, Cambridge, United Kingdom and New York, NY, USA, https://doi.org/10.1017/9781009157896, 2021.

Jacobson, M. Z.: Comment on "Radiative absorption enhancements due to the mixing state of atmospheric black carbon", Science, 339, 393, https://doi.org/10.1126/science.1229920, 2013.

Kang, Z., Ma, P., Quan, J., Liao, Z., Pan, Y., Liu, H., Pan, X., Dou, Y., Zhao, X., Cheng, Z., Wang, Q., Yuan, T., and Jia, X.: Mixing state of refractory black carbon in the residual layer over megacity, Atmos. Environ., 295, 119558, https://doi.org/10.1016/j.atmosenv.2022.119558, 2023.

Li, J., Chen, X., Wang, Z., Du, H., Yang, W., Sun, Y., Hu, B., Li, J., Wang, W., Wang, T., Fu, P., and Huang, H.: Radiative and heterogeneous chemical effects of aerosols on ozone and inorganic aerosols over East Asia, Sci. Total Environ., 622–623, 1327–1342, https://doi.org/10.1016/j.scitotenv.2017.12.041, 2018.

Li, J., Han, Z., Wu, Y., Xiong, Z., Xia, X., Li, J., Liang, L., and Zhang, R.: Aerosol radiative effects and feedbacks on boundary layer meteorology and $PM_{2.5}$ chemical components during winter haze events over the Beijing-Tianjin-Hebei region, Atmos. Chem. Phys., 20, 8659–8690, https://doi.org/10.5194/acp-20-8659-2020, 2020.

Li, M., Liu, H., Geng, G. N., Hong, C. P., Liu, F., Song, Y., Tong, D., Zheng, B., Cui, H. Y., Man, H. Y., Zhang, Q., and He, K. B.: Anthropogenic emission inventories in China: a review, Natl. Sci. Rev., 4, 834–866, https://doi.org/10.1093/nsr/nwx150, 2017.

Li, W., Shao, L., Zhang, D., Ro, C.-U., Hu, M., Bi, X., Geng, H., Matsuki, A., Niu, H., and Chen, J.: A review of single aerosol particle studies in the atmosphere of East Asia: morphology, mixing state, source, and heterogeneous reactions, J. Clean. Prod., 112, 1330–1349, https://doi.org/10.1016/j.jclepro.2015.04.050, 2016.

Li, W., Riemer, N., Xu, L., Wang, Y., Adachi, K., Shi, Z., Zhang, D., Zheng, Z., and Laskin, A.: Microphysical properties of atmospheric soot and organic particles: measurements, modeling, and impacts, npj Clim. Atmos. Sci., 7, 65, https://doi.org/10.1038/s41612-024-00610-8, 2024.

Lin, P., Hu, M., Deng, Z., Slanina, J., Han, S., Kondo, Y., Takegawa, N., Miyazaki, Y., Zhao, Y., and Sugimoto, N.: Seasonal and diurnal variations of organic carbon in $PM_{2.5}$ in Beijing and the estimation of secondary organic carbon, J. Geophys. Res.-Atmos., 114, D00G11, https://doi.org/10.1029/2008JD010902, 2009.

Liu, C., Chung, C. E., Yin, Y., and Schnaiter, M.: The absorption Ångström exponent of black carbon: from numerical aspects, Atmos. Chem. Phys., 18, 6259–6273, https://doi.org/10.5194/acp-18-6259-2018, 2018.

Liu, D. T., Whitehead, J., Alfarra, M. R., Reyes-Villegas, E., Spracklen, D. V., Reddington, C. L., Kong, S. F., Williams, P. I., Ting, Y. C., Haslett, S., Taylor, J. W., Flynn, M. J., Morgan, W. T., McFiggans, G., Coe, H., and Allan, J. D.: Black-carbon absorption enhancement in the atmosphere determined by particle mixing state, Nat. Geosci., 10, 184–188, https://doi.org/10.1038/Ngeo2901, 2017.

Liu, D. T., He, C. L., Schwarz, J. P., and Wang, X.: Lifecycle of light-absorbing carbonaceous aerosols in the atmosphere, Npj Clim. Atmos. Sci., 3, 40, https://doi.org/10.1038/s41612-020-00145-8, 2020.

Liu, X., Ma, P.-L., Wang, H., Tilmes, S., Singh, B., Easter, R. C., Ghan, S. J., and Rasch, P. J.: Description and evaluation of a new four-mode version of the Modal Aerosol Module (MAM4) within version 5.3 of the Community Atmosphere Model, Geosci. Model Dev., 9, 505–522, https://doi.org/10.5194/gmd-9-505-2016, 2016.

Mann, G. W., Carslaw, K. S., Spracklen, D. V., Ridley, D. A., Manktelow, P. T., Chipperfield, M. P., Pickering, S. J., and Johnson, C. E.: Description and evaluation of GLOMAP-mode: a modal global aerosol microphysics model for the UKCA composition-climate model, Geosci. Model Dev., 3, 519–551, https://doi.org/10.5194/gmd-3-519-2010, 2010.

Matsui, H.: Black carbon simulations using a size- and mixing-state-resolved three-dimensional model: 1. Radiative effects and their uncertainties, J. Geophys. Res.-Atmos., 121, 1793–1807, https://doi.org/10.1002/2015jd023998, 2016.

Matsui, H., Koike, M., Kondo, Y., Fast, J. D., and Takigawa, M.: Development of an aerosol microphysical module: Aerosol Two-dimensional bin module for foRmation and Aging Simulation (ATRAS), Atmos. Chem. Phys., 14, 10315–10331, https://doi.org/10.5194/acp-14-10315-2014, 2014.

Matsui, H., Hamilton, D. S., and Mahowald, N. M.: Black carbon radiative effects highly sensitive to emitted particle size when resolving mixing-state diversity, Nat. Commun., 9, 3446, https://doi.org/10.1038/s41467-018-05635-1, 2018.

Mie, G.: Beiträge zur Optik Trüber Medien, Speziell Kolloidaler Metallösungen, Ann. Phys., 25, 377, https://doi.org/10.1002/andp.19083300302, 1908.

Mishchenko, M. I., Dlugach, J. M., Yanovitskij, E. G., and Zakharova, N. T.: Bidirectional reflectance of flat, optically thick particulate layers: an efficient radiative transfer solution and applications to snow and soil surfaces, J. Quant. Spectrosc. Ra., 63, 409–432, https://doi.org/10.1016/S0022-4073(99)00028-X, 1999.

National Centers for Environmental Prediction/National Weather Service/NOAA/U.S. Department of Commerce: NCEP FNL Operational Model Global Tropospheric Analyses, continuing from July 1999, updated daily, Research Data Archive at the National Center for Atmospheric Research, Computational and Information Systems Laboratory [data set], https://doi.org/10.5065/D6M043C6, 2000.

Obiso, V. and Jorba, O.: Aerosol-radiation interaction in atmospheric models: Idealized sensitivity study of simulated short-wave direct radiative effects to particle microphysical properties, J. Aerosol Sci., 115, 46–61, https://doi.org/10.1016/j.jaerosci.2017.10.004, 2018.

Paasonen, P., Kupiainen, K., Klimont, Z., Visschedijk, A., Denier van der Gon, H. A. C., and Amann, M.: Continental anthropogenic primary particle number emissions, Atmos. Chem. Phys., 16, 6823–6840, https://doi.org/10.5194/acp-16-6823-2016, 2016.

Peng, J., Hu, M., Guo, S., Du, Z., Zheng, J., Shang, D., Levy Zamora, M., Zeng, L., Shao, M., Wu, Y. S., Zheng, J., Wang, Y., Glen, C. R., Collins, D. R., Molina, M. J., and Zhang, R.: Markedly enhanced absorption and direct radiative forcing of black carbon under polluted urban environments, P. Natl. Acad. Sci. USA, 113, 4266–4271, https://doi.org/10.1073/pnas.1602310113, 2016.

Qin, Y. M., Tan, H. B., Li, Y. J., Li, Z. J., Schurman, M. I., Liu, L., Wu, C., and Chan, C. K.: Chemical characteristics of brown carbon in atmospheric particles at a suburban site near Guangzhou, China, Atmos. Chem. Phys., 18, 16409–16418, https://doi.org/10.5194/acp-18-16409-2018, 2018.

Ran, L., Deng, Z. Z., Wang, P. C., and Xia, X. A.: Black carbon and wavelength-dependent aerosol absorption in the North China Plain based on two-year aethalometer measurements, Atmos. Environ., 142, 132–144, https://doi.org/10.1016/j.atmosenv.2016.07.014, 2016.

Riemer, N., West, M., Zaveri, R. A., and Easter, R. C.: Simulating the evolution of soot mixing state with a particle-resolved aerosol model, J. Geophys. Res.-Atmos., 114, D09202, https://doi.org/10.1029/2008jd011073, 2009.

Riemer, N., P. Ault, A., West, M., L. Craig, R., and H. Curtis, J.: Aerosol Mixing State: Measurements, Modeling, and Impacts, Rev. Geophys., 57, 187–249, https://doi.org/10.1029/2018RG000615, 2019.

Shen, W. X., Wang, M. H., Riemer, N., Zheng, Z. H., Liu, Y. W., and Dong, X. Y.: Improving BC Mixing State and CCN Activity Representation With Machine Learning in the Community Atmosphere Model Version 6 (CAM6), J. Adv. Model. Earth Sy., 16, e2023MS003889, https://doi.org/10.1029/2023MS003889, 2024.

Stevens, R. and Dastoor, A.: A Review of the Representation of Aerosol Mixing State in Atmospheric Models, Atmosphere, 10, 168, https://doi.org/10.3390/atmos10040168, 2019.

Sun, J., Xie, C., Xu, W., Chen, C., Ma, N., Xu, W., Lei, L., Li, Z., He, Y., Qiu, Y., Wang, Q., Pan, X., Su, H., Cheng, Y., Wu, C., Fu, P., Wang, Z., and Sun, Y.: Light absorption of black carbon and brown carbon in winter in North China Plain: comparisons between urban and rural sites, Sci. Total Environ., 770, 144821, https://doi.org/10.1016/j.scitotenv.2020.144821, 2021.

Toon, O. B. and Ackerman, T. P.: Algorithms for the calculation of scattering by stratified spheres, Appl. Opt., 20, 3657–3660, https://doi.org/10.1364/AO.20.003657, 1981.

Tuccella, P., Curci, G., Pitari, G., Lee, S., and Jo, D. S.: Direct Radiative Effect of Absorbing Aerosols: Sensitivity to Mixing State, Brown Carbon, and Soil Dust Refractive Index and Shape, J. Geophys. Res.-Atmos., 125, e2019JD030967, https://doi.org/10.1029/2019JD030967, 2020.

Wang, J., Liu, D., Ge, X., Wu, Y., Shen, F., Chen, M., Zhao, J., Xie, C., Wang, Q., Xu, W., Zhang, J., Hu, J., Allan, J., Joshi, R., Fu, P., Coe, H., and Sun, Y.: Characterization of black carbon-containing fine particles in Beijing during wintertime, Atmos. Chem. Phys., 19, 447–458, https://doi.org/10.5194/acp-19-447-2019, 2019.

Wang, Y., Li, W., Huang, J., Liu, L., Pang, Y., He, C., Liu, F., Liu, D., Bi, L., Zhang, X., and Shi, Z.: Nonlinear Enhancement of Radiative Absorption by Black Carbon in Response to Particle Mixing Structure, Geophys. Res. Lett., 48, e2021GL096437, https://doi.org/10.1029/2021gl096437, 2021a.

Wang, Y. Y., Pang, Y. E., Huang, J., Bi, L., Che, H. Z., Zhang, X. Y., and Li, W. J.: Constructing Shapes and Mixing Structures of Black Carbon Particles With Applications to Optical Calculations, J. Geophys. Res.-Atmos., 126, e2021JD034620, https://doi.org/10.1029/2021JD034620, 2021b.

Wang, Y., Hu, R., Wang, Q., Li, Z., Cribb, M., Sun, Y., Song, X., Shang, Y., Wu, Y., Huang, X., and Wang, Y.: Different effects of anthropogenic emissions and aging processes on the mixing state of soot particles in the nucleation and accumulation modes, Atmos. Chem. Phys., 22, 14133–14146, https://doi.org/10.5194/acp-22-14133-2022, 2022.

Wang, Z. F., Maeda, T., Hayashi, M., Hsiao, L. F., and Liu, K. Y.: A nested air quality prediction modeling system for urban and regional scales: Application for high-ozone episode in Taiwan, Water Air Soil Poll., 130, 391–396, https://doi.org/10.1023/A:1013833217916, 2001.

Wu, Y., Zhang, R., Tian, P., Tao, J., Hsu, S. C., Yan, P., Wang, Q., Cao, J., Zhang, X., and Xia, X.: Effect of ambient humidity on the light absorption amplification of black carbon in Beijing during January 2013, Atmos. Environ., 124, 217–223, https://doi.org/10.1016/j.atmosenv.2015.04.041, 2016.

Wu, Y., Xia, Y., Zhou, C., Tian, P., Tao, J., Huang, R.-J., Liu, D., Wang, X., Xia, X., Han, Z., and Zhang, R.: Effect of source variation on the size and mixing state of black carbon aerosol in urban Beijing from 2013 to 2019: Implication on light absorption, Environ. Pollut., 270, 116089, https://doi.org/10.1016/j.envpol.2020.116089, 2021.

Xie, C., Xu, W., Wang, J., Wang, Q., Liu, D., Tang, G., Chen, P., Du, W., Zhao, J., Zhang, Y., Zhou, W., Han, T., Bian, Q., Li, J., Fu, P., Wang, Z., Ge, X., Allan, J., Coe, H., and Sun, Y.: Vertical characterization of aerosol optical properties and brown carbon in winter in urban Beijing, China, Atmos. Chem. Phys., 19, 165–179, https://doi.org/10.5194/acp-19-165-2019, 2019.

Xie, X., Hu, J., Qin, M., Guo, S., Hu, M., Ji, D., Wang, H., Lou, S., Huang, C., Liu, C., Zhang, H., Ying, Q., Liao, H., and Zhang, Y.: Evolution of atmospheric age of particles and its implications for the formation of a severe haze event in eastern China, Atmos. Chem. Phys., 23, 10563–10578, https://doi.org/10.5194/acp-23-10563-2023, 2023.

Xu, P., Chen, Y., and Ye, X.: Haze, air pollution, and health in China, Lancet, 382, 2067, https://doi.org/10.1016/S0140-6736(13)62693-8, 2013.

Yang, W., Li, J., Wang, W., Li, J., Ge, M.-F., Sun, Y., Chen, X., Ge, B., Tong, S., Wang, Q., and Wang, Z.: Investigating secondary organic aerosol formation pathways in China during 2014, Atmos. Environ., 213, 133–147, https://doi.org/10.1016/j.atmosenv.2019.05.057, 2019.

Yao, Y., Curtis, J. H., Ching, J., Zheng, Z., and Riemer, N.: Quantifying the effects of mixing state on aerosol optical properties, Atmos. Chem. Phys., 22, 9265–9282, https://doi.org/10.5194/acp-22-9265-2022, 2022.

Yu, F. and Luo, G.: Simulation of particle size distribution with a global aerosol model: contribution of nucleation to aerosol and CCN number concentrations, Atmos. Chem. Phys., 9, 7691–7710, https://doi.org/10.5194/acp-9-7691-2009, 2009.

Yu, F., Luo, G., and Ma, X.: Regional and global modeling of aerosol optical properties with a size, composition, and mixing state resolved particle microphysics model, Atmos. Chem. Phys., 12, 5719–5736, https://doi.org/10.5194/acp-12-5719-2012, 2012.

Yu, P., Toon, O., Bardeen, C., Mills, M., Fan, T., English, J., and Neely, R.: Evaluations of Tropospheric Aerosol Properties Simulated by the Community Earth System Model with a Sectional Aerosol Microphysics Scheme, J. Adv. Model. Earth Sy., 7, 865–914, https://doi.org/10.1002/2014MS000421, 2015.

Yus-Díez, J., Bernardoni, V., Močnik, G., Alastuey, A., Ciniglia, D., Ivančič, M., Querol, X., Perez, N., Reche, C., Rigler, M., Vecchi, R., Valentini, S., and Pandolfi, M.: Determination of the multiple-scattering correction factor and its cross-sensitivity to scattering and wavelength dependence for different AE33 Aethalometer filter tapes: a multi-instrumental approach, Atmos. Meas. Tech., 14, 6335–6355, https://doi.org/10.5194/amt-14-6335-2021, 2021.

Zaveri, R. A., Barnard, J. C., Easter, R. C., Riemer, N., and West, M.: Particle-resolved simulation of aerosol size, composition, mixing state, and the associated optical and cloud condensation nuclei activation properties in an evolving urban plume, J. Geophys. Res.-Atmos., 115, D17210, https://doi.org/10.1029/2009jd013616, 2010.

Zhang, H., Guo, H., Hu, J., Ying, Q., and Kleeman, M. J.: Modeling atmospheric age distribution of elemental carbon using a regional age-resolved particle representation framework, Environ. Sci. Technol., 53, 270–278, https://doi.org/10.1021/acs.est.8b05895, 2019.

Zhang, Y., Liu, H., Lei, S., Xu, W., Tian, Y., Yao, W., Liu, X., Liao, Q., Li, J., Chen, C., Sun, Y., Fu, P., Xin, J., Cao, J., Pan, X., and Wang, Z.: Mixing state of refractory black carbon in fog and haze at rural sites in winter on the North China Plain, Atmos. Chem. Phys., 21, 17631–17648, https://doi.org/10.5194/acp-21-17631-2021, 2021.

Zhao, G., Shen, C., and Zhao, C.: Technical note: Mismeasurement of the core-shell structure of black carbon-containing ambient aerosols by SP2 measurements, Atmos. Environ., 243, 117885, https://doi.org/10.1016/j.atmosenv.2020.117885, 2020.

Zhao, G., Tan, T., Zhu, Y., Hu, M., and Zhao, C.: Method to quantify black carbon aerosol light absorption enhancement with a mixing state index, Atmos. Chem. Phys., 21, 18055–18063, https://doi.org/10.5194/acp-21-18055-2021, 2021.

Zhao, G., Tan, T., Hu, S., Du, Z., Shang, D., Wu, Z., Guo, S., Zheng, J., Zhu, W., Li, M., Zeng, L., and Hu, M.: Mixing state of black carbon at different atmospheres in north and southwest China, Atmos. Chem. Phys., 22, 10861–10873, https://doi.org/10.5194/acp-22-10861-2022, 2022.

Zhao, P., Dong, F., Yang, Y., He, D., Zhao, X., Zhang, W., Yao, Q., and Liu, H.: Characteristics of carbonaceous aerosol in the region of Beijing, Tianjin, and Hebei, China, Atmos. Environ., 71, 389–398, https://doi.org/10.1016/j.atmosenv.2013.02.010, 2013.

Zheng, G. J., Duan, F. K., Su, H., Ma, Y. L., Cheng, Y., Zheng, B., Zhang, Q., Huang, T., Kimoto, T., Chang, D., Pöschl, U., Cheng, Y. F., and He, K. B.: Exploring the severe winter haze in Beijing: the impact of synoptic weather, regional transport and heterogeneous reactions, Atmos. Chem. Phys., 15, 2969–2983, https://doi.org/10.5194/acp-15-2969-2015, 2015.

Zheng, H., Kong, S., Chen, N., and Wu, C.: Secondary inorganic aerosol dominated the light absorption enhancement of black carbon aerosol in Wuhan, Central China, Atmos. Environ., 287, 119288, https://doi.org/10.1016/j.atmosenv.2022.119288, 2022.

Zhou, C. H., Gong, S., Zhang, X. Y., Liu, H. L., Xue, M., Cao, G. L., An, X. Q., Che, H. Z., Zhang, Y. M., and Niu, T.: Towards the improvements of simulating the chemical and optical properties of Chinese aerosols using an online coupled model – CUACE/Aero, Tellus B, 64, 91–102, 2012.